Biosensors and Bioelectronics 147 (2020) 111789

Contents lists available at ScienceDirect

Biosensors and Bioelectronics

journal homepage: http://www.elsevier.com/locate/bios

Electrochemiluminescence biosensor for miRNA-21 based on toehold-mediated strand displacement amplification with $Ru(phen)_3^{2+}$ loaded DNA nanoclews as signal tags

Ying Zhang [a], Guoyan Xu [b], Guili Lian [b], Fang Luo [d], Qunfang Xie [b,**], Zhenyu Lin [c,*], Guonan Chen [c]

[a] Central Laboratory, The First Affiliated Hospital of Fujian Medical University, Fuzhou, Fujian, 350005, China
[b] Department of Cadre's Ward, The First Affiliated Hospital of Fujian Medical University, Fuzhou, Fujian, 350005, China
[c] Ministry of Education Key Laboratory for Analytical Science of Food Safety and Biology, Fujian Provincial Key Laboratory of Analysis and Detection for Food Safety, College of Chemistry, Fuzhou University, Fuzhou, Fujian, 350116, China
[d] College of Biological Science and Engineering, Fuzhou University, Fuzhou, Fujian, 350116, China

ARTICLE INFO

Keywords:
Electrochemiluminescence biosensor
miRNA-21
Toehold-mediated strand displacement
DNA nanoclews
$Ru(phen)_3^{2+}$

ABSTRACT

A novel electrochemiluminescence (ECL) biosensor was developed for high sensitive and selective detection of miRNA-21 based on the efficient and specific toehold-mediated strand displacement (TMSD) amplification with $Ru(phen)_3^{2+}$ loaded DNA nanoclews (NCs–$Ru(phen)_3^{2+}$) as signal tags. The stable DNA nanoclews, synthesized by a simple rolling circle amplification reaction, were employed to load with $Ru(phen)_3^{2+}$ efficiently as ECL signal tags to amplify the signals. As for TMSD, the substrate strand (Sub) was initially hybridized with P1 and P2 to form DNA duplex structures with a toehold 1. miRNA-21 could hybridize with the toehold 1 and trigger the TMSD amplification with the help of assist strand, releasing lots of P1 stands from DNA duplex structures. The TMSD technique realized the converting and amplification of the single miRNA-21 input to lots of output DNA (namely P1) with good selectivity, simultaneously. Output P1 were designed to expand the stem-locked region of HP, which were immobilized on the Au electrodes firstly. Subsequently, the opened HP could hybridize with the $Ru(phen)_3^{2+}$, capturing the ECL signal tags closed to the sensing surface. The ECL intensity of the system had a linear relationship with the logarithm of the miRNA-21 concentration in the range of 1.0 fM to 100 pM with a limit of detection of 0.65 fM. The strategy was further applied to detect miRNA-21 in complex samples, and the result was consistent with the qRT-PCR.

1. Introduction

MicroRNAs (miRNAs), a class of endogenous and short noncoding RNAs, are known to be significant regulators of gene expression (Bartel, 2004; He and Hannon, 2004) and their abnormal expression is associated with different diseases, containing cancers, cardiovascular disease and neurological disease, and so on (Di Leva and Croce, 2013; Lujambio and Lowe, 2012; Small and Olson, 2011). So which has been regarded as potential biomarkers for early clinically diagnostic. Since miRNAs hold the characteristics of low abundance and highly homologous sequences, the methods developed for miRNAs detection need have the characters of high sensitivity and selectivity. A series of powerful amplification strategies, such as real-time polymerase chain reaction (RT-PCR) (Kulcheski et al., 2010; Raymond et al., 2005), rolling circle amplification (Cheng et al., 2009; Zhang et al., 2015) and exponential amplification (Wang and Zhang, 2012; Yu et al., 2014) have been coupled with different detection technologies (such as fluorescence, electrochemistry, and so on) to realize sensitive and selective miRNAs detection.

Electrochemiluminescence (ECL) detection has the advantages of extremely high sensitivity, wide dynamic range, low background signal and simple equipment (Babarniri et al., 2019; Cao et al. 2018, 2019; Chen et al., 2017; Li et al., 2017a; Rizwan et al., 2018). Many sensitive ECL biosensors have been developed for miRNAs and DNA detection. For examples, Xu et al. proposed an ECL regenerated biosensor for the

* Corresponding author. 2 Xue Yuan Road, University Town Fuzhou, Fujian, PR China.
** Corresponding author. No.20 Chazhong Road, Fuzhou, Fujian, PR China.
E-mail addresses: xqf504@163.com (Q. Xie), zylin@fzu.edu.cn (Z. Lin).

https://doi.org/10.1016/j.bios.2019.111789
Received 2 September 2019; Received in revised form 12 October 2019; Accepted 15 October 2019
Available online 17 October 2019

detection of miRNA based on the 3D DNA walking machine, and distance-controllable signal quenching and enhancing by CdS:Mn QDs and AuNPs (Xu et al., 2017). Wang et al. (2018) reported a nano polythionine-based ECL biosensor for the $p16^{INK4a}$ gene detection using core-shell luminescent nanocomposites as ECL labels (Wang et al., 2018). These methods exhibited good sensitivity, but the preparation and label of ECL reports were time consuming. Hence, it is necessary to find out some way to address these problems.

DNA nanoclews (DNA NCs) can be synthesized by the self-assembly of RCA products, which are generated by only two DNA strands (one primer and one palindromic sequence coded template). Which has been widely applied in drug delivery including small-molecule drugs, proteins, CpG oligodeoxynucleotides and small interfering RNA (siRNA) (Kim et al., 2017; Sun et al. 2014, 2015; Wang et al., 2017). Recently, DNA NCs has been applied to develop ECL biosensor with high sensitivity. For example, Yuan's group reported an ECL aptasensor based on a novel ECL signal tags of DNA nanoflowers (NFs) and target conversion strategy for mucin 1 detection (Li et al., 2017b). The DNA NFs in situ generated by RCA, and the ECL luminophore of Dox-ABEI complex was embedded into the dsDNA structures of DNA NFs to generate increased ECL signals. $Ru(phen)_3^{2+}$ is a common luminophore with high ECL emission efficiency, which could be intercalated into the grooves of DNA duplex with high affinity. Several ECL biosensors based on hyperbranched rolling circle amplification (HRCA) using the $Ru(phen)_3^{2+}$ as luminophore has been reported since the product of HRCA contains large amount of DNA duplex structures (Yang et al., 2016; Zhang et al., 2017). Because DNA NCs are made of DNA duplex structures, $Ru(phen)_3^{2+}$ can be loaded on the DNA NCs also and act as ECL signal tags (NCs–$Ru(phen)_3^{2+}$).

Toehold-mediated strand displacement (TMSD) is a kind of enzyme-free isothermal amplification technique, showing good selectivity and sensitivity. The toehold of TMSD usually consists of 5–8 nucleotides, which initiates hybridization by exposed toehold parts with a spot of target gene, resulting in strand displacement and signal amplification (Srinivas et al., 2013; Zhang and Seelig, 2011; Zhu et al., 2013). miRNA-21 is a well-known oncogenic miRNA with overexpression in various cancers (Zhu et al., 2008), and was selected as a target. In this study, an ultrasensitive and good selective ECL biosensor has been developed for miRNA-21 detection based on TMSD amplification using NCs–$Ru(phen)_3^{2+}$ as signal tags. The schematic illustrating of the ECL biosensor is shown in Scheme 1. Initially, the DNA NCs were simply prepared by RCA with palindromic sequences encoded primers to generate clewlike shape nanostructures (Scheme 1A). Stable ECL signal tags (NCs–$Ru(phen)_3^{2+}$) were obtained by the incubation of DNA NCs with $Ru(phen)_3^{2+}$. Lots of $Ru(phen)_3^{2+}$ were embedded into the DNA duplex structures of DNA NCs to amplified the ECL signal of system. Meanwhile, the pre-preparation of NCs–$Ru(phen)_3^{2+}$ could simplify the experimental procedure. As depicted in Scheme 1B, the substrate strand (Sub) hybridized with probe 1 (P1) and probe 2 (P2) to form DNA duplex structure with exposing toehold 1. In the presence of target miRNA-21 and assist strand, the miRNA-21 bound to the toehold 1 and displaced P2 from sub strand via TMSD amplification to expose toehold 2. The assist strand hybridized with the toehold 2 and liberated the P1 and miRNA-21, subsequently. Simultaneously, the released miRNA-21 could bind to the DNA duplex structure again, which induced a cyclic reaction. After numerous cycles, the sensing strategy could realize the converting of "the single miRNA-21 molecule to lots of output DNA (P1)" and lead to signal amplification. P1 was designed to expand the stem-locked region of HP which was immobilized on the Au electrodes via Au–S bond. And the opened HP with sequence of 5′-CCGGCAAGCTGCCCGTGCCC-3′ could be hybridized with NCs–$Ru(phen)_3^{2+}$ containing the complementary sequence (5′-GGGCACGGGCAGCTTGCCGG-3′) to capture the signal tags close to the sensing surface. The relevant detailed sequence information was exhibited in Table S1 in the supplemental information (SI). With increasing concentration of miRNA-21, more released P1 bound to the HP and more NCs–$Ru(phen)_3^{2+}$ were captured on the electrode surface, causing increased ECL intensity. On account of the stabilized NCs–$Ru(phen)_3^{2+}$ signal tags and versatile TMSD strategy, this proposed miRNA sensing platform exhibited highly sensitivity, good selectivity, and could be applied for the real samples assay. Significantly, the strategy was programmable, so multiple sequences of miRNA detection might be achieved with simple sequence design.

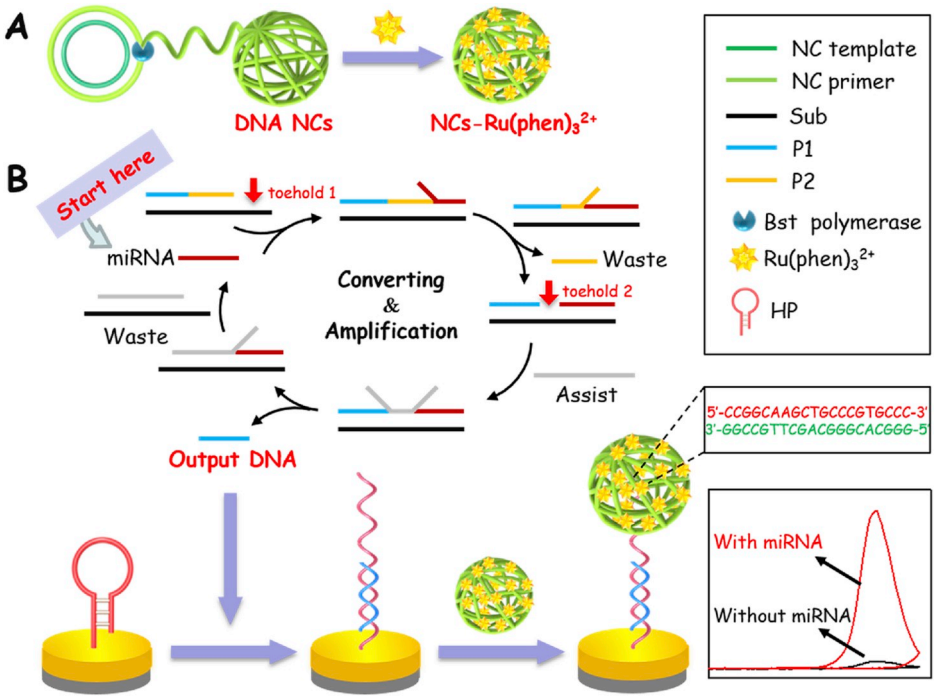

Scheme 1. Schematic illustration of the ECL biosensor for miRNA-21 quantitative analysis.

2. Experimental section

2.1. Synthesis and preparation of DNA NCs

DNA NCs were synthesized according to the previous reports (Sun et al., 2015). Initially, the 5′ phosphorylated single-stranded DNA templates (NC templates) were cyclized by CircLigase II ssDNA ligase kit. Namely, NC templates (0.5 μM) were added into a 40 μL reaction solution containing CircLigase II ssDNA ligase (5.0 U/μL), $MnCl_2$ (2.5 mM), betaine (1 M), and the solution was incubated at 60 °C for 1 h. Subsequently, the non-ligatured NC templates were removed by Exo I (0.5 U/μL) and Exo III (1.0 U/μL) at 37 °C for 1 h and heated at 80 °C for 15 min. The circular NC templates were hybridized with NC primers (0.5 μM) to trigger the RCA reaction at 63 °C for 17 h in 100 μL of the amplification solution including dNTPs (0.4 mM), 10 × BSA (2 μL), Bst DNA polymerase (0.08 U/μL) and its 1 × buffer. The obtained DNA NCs were purified by DNA Clean-Up kit and dissolved in the buffer 1.

2.2. $Ru(phen)_3^{2+}$ loaded DNA NCs

The depurative DNA NCs (10 μL) were mixed with $Ru(phen)_3^{2+}$ (1.0 μL, 10 mM) in buffer 1 (380 μL), and the mixed solution was incubated at 4 °C for 3 h to allow $Ru(phen)_3^{2+}$ to be embedded in DNA NCs as ECL signal tag (NCs–$Ru(phen)_3^{2+}$). The above solution was transferred to an Amicon ultra 3 K device to filter the superfluous $Ru(phen)_3^{2+}$ with centrifugal speed of 14,000×*g* for 20 min. The prepared NCs–$Ru(phen)_3^{2+}$ were stored at 4 °C for further studies.

2.3. TMSD strategy

The mixture containing substrate strand (Sub) (4.0 μM), P1 (8.0 μM) and P2 (8.0 μM) were heated to 90 °C for 10 min, and cooled down to room temperature getting the DNA duplex structure with a toehold 1. And then, the DNA duplex (10 μL) was mixed with the assist (0.8 μM) and the target miRNA diluted in different concentrations at 37 °C for 3 h, and the TMSD was proceed.

2.4. Construction and measurement of the ECL biosensor

Prior to the electrode modification, the Au electrode was polished with alumina power and then sonicated in ethyl alcohol absolute and ultrapure water. The well-polished Au electrode was activated by cycling the potential between 0 and 1.2 V in H_2SO_4 (0.5 M) until a stable cyclic voltammetry obtained. The thiolated HP (2.0 μM) was firstly dissolved with buffer 2 containing 1 mM DTT overnight at room temperature to cleave the disulfide bond, and then dropped on the cleaned Au electrode surface. After incubation for 2 h at 37 °C, the HP was covalently bound to Au electrode via the Au–S binding. To remove the nonspecific adsorption, MCH (1.0 mM) was added into the electrode for 30 min. And the aforementioned amplification solution was added into the modified Au electrode at 37 °C for 1 h. After being rinsed and dried, the prepared NCs–$Ru(phen)_3^{2+}$ was dropped on the modified Au electrode surface and allowed to react 2 h at 37 °C. Then the ECL measurement was carried out with potential of 0.6 V–1.6 V and scan speed of 100 mV/s in 2.0 mL of phosphate buffer saline (PBS, 100 mM, pH 7.4) containing 20 mM TPA. The voltage of the photomultiplier tube was set at −800 V.

3. Results and discussion

3.1. Characterization of DNA NCs

An agarose gel electrophoresis was implemented to validate the formation of DNA NCs (Fig. 1(A)). As seen from lane NC, a clear band was observed at the initial site of this lane. SYBR Green I was mixed with the DNA NCs to insert into the groove of DNA duplex, and thus produced enhanced fluorescent signal. As shown in Fig. 1(B), the fluorescence spectra demonstrated the synthetic DNA NCs contained the DNA duplex. Additionally, the morphologies of DNA NCs were investigated by the scanning electron microscope (SEM). As seen from Fig. 1(C), the DNA NCs exhibited a uniform and nearly spherical nanostructure, and the average size was ~100 nm in diameter. The zeta potential analysis (Fig. 1(D)) showed a negative potential of −39.5 mV of DNA NCs, which can be owned to the negatively charged phosphate on the molecular skeleton. After incubation with the positively charged $Ru(phen)_3^{2+}$ which can insert to the DNA NCs, the zeta potential changed to −5.9 mV indicating the successful preparation of ECL signal tags (NCs–$Ru(phen)_3^{2+}$).

The stability of NCs–$Ru(phen)_3^{2+}$ was studied as well with different storage time of fresh one (0 day), 0.5 day, 1 day, 3 days, 7 days, 30 days, and 90 days at 4 °C. As shown in Fig. 1(E), the recorded ECL signal had no significant difference manifesting the good stability of the prepared

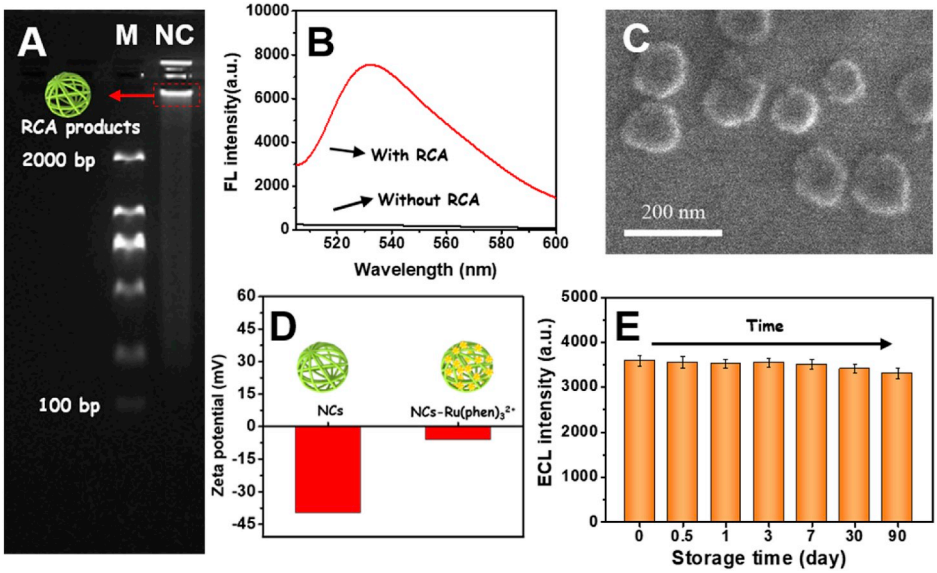

Fig. 1. (A) Agarose gel electrophoresis of DNA NCs. (B) Fluorescence spectra of DNA NCs mixed with SYBR Green I. (C) TEM images of DNA NCs. (D) Zeta potential characterization of DNA NCs and $Ru(phen)_3^{2+}$ embedded DNA NCs. (E) The stability study of DNA NCs which were stored at 4 °C with different storage times.

NCs–Ru(phen)$_3^{2+}$.

3.2. Feasibility of the proposed sensing platform

To verify the validity of TMSD strategy, the products were analyzed by polyacrylamide gel electrophoresis also. As shown in Fig. 2(A), the Sub-P1-P2 (lane c) was formed by the hybridization between the Sub, P1 and P2. It migrated more slowly than the single Sub strand (lane a) and the band generated by hybridization of Sub and P1 (lane b). After the addition of assist strands, the band did not show significant change in the control group (Fig. 2(A), lane d). At the presence of target miRNA-21, a well-defined band was observed at the bottom of lane f, suggesting that miRNA-21 was converted to lots of P1. Briefly, the TMSD was initiated and efficient. However, inconspicuous band was appeared without the assist strands as shown in lane e in Fig. 2(A). It was speculated that small amount of P2 was replaced but the P1 was not, owing to lack of the help of assist. The above results verified the successful fabrication of TMSD strategy.

The nyquist diagrams were employed to characterize the stepwise assembly process of electrodes. The charge transfer resistance (R_{et}) equals the semicircle diameter, which directly reflects the transfer kinetics of the $[Fe(CN)_6]^{3-/4-}$ at the electrode surface. As shown in Fig. 2 (B), HP modified Au electrode (curve b) exhibited an obvious higher R_{et} compared to that of bare Au electrode (curve a), on account of the electrostatic repulsion between the $[Fe(CN)_6]^{3-/4-}$ and negatively charged phosphate backbone of HP. This result indicated that HP strands were successfully immobilized on the surface of Au electrodes via Au–S bond. After the blocking of MCH on the electrode, the R_{et} increased obviously (curve c) because the formation of a compact layer by MCH that hindered the electron transfer to a great extent. Subsequently, the addition of released P1 by the TMSD strategy caused inconspicuous decrease of R_{et} (curve d), which could be explained that the stem-locked region of HP were expanded by P1. Then, the R_{et} increased significantly with the incubation of NCs–Ru(phen)$_3^{2+}$ (curve e), implying the successful capture of ECL signal tags by the opened HP. These results suggested the assembly process on the surface of the gold electrode was consistent with the designed principle.

The feasibility of the ECL sensing platform for miRNA-21 detection was further investigated by recording corresponding ECL signals. Fig. 2 (C) showed the ECL response and the corresponding cyclic voltammogram (CV) curves (inset figure in Fig. 2 (C)) with and without the addition of the target. Only weak ECL signal (curve a) and anodic current of Ru(phen)$_3^{2+}$ oxidation (curve a') were observed at the absence of target miRNA-21. However, after the introduction of miRNA-21, significantly enhancement in ECL intensity was detected (curve b), and the corresponding CV curve displayed the typical obvious oxidation peak attributed to the oxidation of Ru(phen)$_3^{2+}$ (curve b'). The obvious increased ECL signal was due to that (i) the target miRNA-21 could induce the process of TMSD by the hybridization and strand displacement, (ii) lots of P1 were released from TMSD reaction to open HP immobilized on the surface of electrodes, (iii) and hence the NCs–Ru(phen)$_3^{2+}$ ECL signal tags were captured onto the sensing interface by the opened HP. These results indicated the presence of target miRNA could amplify ECL signal, namely the proposed sensing platform was practicable.

3.3. Optimization of the experimental conditions

To achieve better performance of the biosensor, the relevant experimental conditions were optimized. Initially, the size of DNA NCs assembly could be influenced by the RCA reaction time easily. The DNA NCs obtained from four RCA reaction times (3 h, 10 h, 17 h, 24 h, respectively) were characterized by the transmitted electron microscopy (TEM). As shown in Figs. S1(A) and (B), (C), (D) in SI, the synthesized DNA NCs were monodisperse and exhibited spherical-like nanostructures with sizes of about 50 nm, 80 nm, 100 nm, and 100 nm, respectively. The sizes of DNA NCs increased with increasing time of RCA, and a longer reaction time did not cause any obvious variation after 17 h. Subsequently, the dynamic light scattering (DLS) were also used to measure the sizes distribution of prepared DNA NCs, and revealed the consistent results (the insets of Figs. S1(A) and (B), (C), (D) in SI). Then, the four sizes of NCs–Ru(phen)$_3^{2+}$ were acted as ECL signal tags for the detection of miRNA-21. As shown in Fig. S1(E) in SI, the results showed that the ECL intensity of the system increased with the

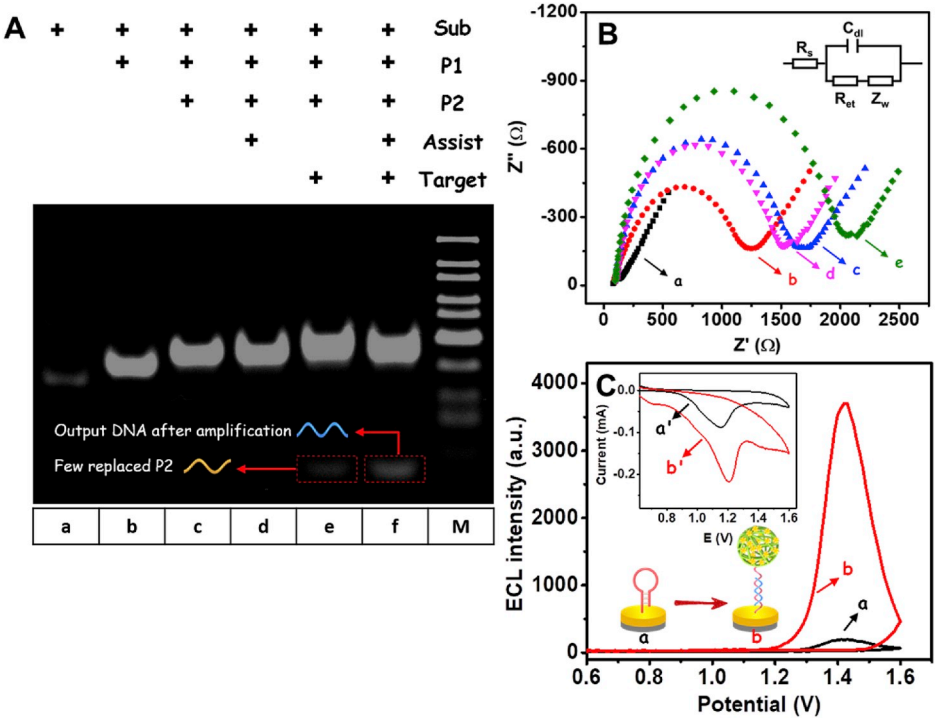

Fig. 2. (A) Polyacrylamide gel electrophoresis analysis of different conditions: (a) Sub, (b) 'a' + P1, (c) 'b' + P2, (d) 'c' + assist, (e) 'c' + miRNA-21, (f) 'c' + miRNA-21 + assist. (B) Nyquist diagrams of different electrodes: (a) bare Au electrode, (b) electrode 'a' + HP, (c) electrode 'b' + MCH, (d) electrode 'c' + released P1, (e) electrode 'd' + NCs–Ru(phen)$_3^{2+}$ in 5.0 mM $[Fe(CN)_6]^{3-/4-}$ including 100 mM KCl. (C) ECL response of the proposed biosensor in the (a) absence and (b) presence of 0.1 pM miRNA-21. The inset figure is the corresponding CV curves. (ECL measurement was carried out with potential of 0.6 V–1.6 V and scan speed of 100 mV/s in 2.0 mL of phosphate buffer saline (PBS, 100 mM, pH 7.4) containing 20 mM TPA. The voltage of the photomultiplier tube was set at −800 V).

increasing of the DNA NCs obtained by RCA reaction time firstly and after 17 h which reached a plateau, so 17 h was chosen in the following study. It is reasonable to speculate that the larger size of DNA NCs can load the higher efficiency of $Ru(phen)_3^{2+}$, hence producing a stronger ECL signal.

The concentration of HP immobilized on the surface of the gold electrode, which could be opened by the released P1 and used to capture the NCs–$Ru(phen)_3^{2+}$ directly influenced the generated ECL signal, which was initially optimized. As shown in Fig. S2(A) in SI, the *ΔECL* (the ECL intensity variation without and with the target) increased along with the HP concentration up to 2.0 μM and then became flat. Therefore, 2.0 μM was chosen as the optimal HP concentration.

The concentration of P1 forming DNA duplex structure (composed of sub, P1 and P2) is critical for signal amplification. Excess P1 would be free in solution and cause the open of the beacon of HP, resulting in background signal, whereas less P1 would lead to low sensitivity of the sensing method. As shown in Fig. S2(B) in SI, the maximum ECL response was achieved at 2.0 μM P1, and then *ΔECL* gradually decreased, which was mainly due to the increased background signal causing by the excessive P1. So, 2.0 μM P1 was used for the following experiment. Likewise, the assist strand was involved in the TMSD process, and hence its concentration was optimized as well. As displayed in Fig. S2(C) in SI, the *ΔECL* enhanced steeply with the increase of assist concentration from 0 to 1.0 μM and then reached a plateau, indicating 1.0 μM of assist was sufficient in this experiment.

Subsequently, the effect of incubation time to capture NCs–Ru $(phen)_3^{2+}$ on the electrode surface was investigated. As shown in Fig. S2 (D) in SI, the ΔECL increased with longer incubation time and reached a plateau after 120 min. Therefore, 120 min was chosen as the optimum captured time.

3.4. Analytical performance of the ECL biosensor

Under the optimal conditions, the ECL signal of proposed biosensor in response to different concentrations of miRNA-21 was investigated. As exhibited in Fig. 3(A), there was quite strong relativity between the ECL intensity and the concentrations of target. Fig. 3(B) depicted that the *ΔECL* was proportional to the logarithm of miRNA-21 concentration from 1.0 fM to 100 pM. The resulting regression equation of the biosensor expressed as:

$$\Delta ECL = 5557 + 1669 \lg C \; R^2 = 0.994 \quad (1)$$

where *C* was the miRNA-21 concentration, and the R^2 was the correlation coefficient. The limit of detection (LOD) was calculated to be 0.65 fM (LOD = 3s/k, where k is the slope of calibration curve and s is the standard deviations of the blank). As exhibited in Table S2 in SI, the developed platform had lower detection limit and much wider concentration range toward miRNA detection compared to some other reported methods. The proposed ECL biosensor exhibited the good sensitivity, which could be attributed to the target induced TMSD strategy and the efficiently $Ru(phen)_3^{2+}$ loaded DNA NCs for signal amplification.

3.5. Selectivity and reproducibility of the ECL biosensor

The ECL responses of the sensing platform toward single-base mismatched miRNA (SM), two-bases mismatched miRNA (TM), miRNA-144, miRNA-122a, and miRNA-32 (as interferents) were used to estimate the selectivity of the developed method. The concentration of interferents were set 1.0 pM, and the target miRNA-21 was 0.10 pM. As shown in Fig. 4(A), the responses from miRNA-21 and the mixture including miRNA-21 displayed quite strong ECL signals. While the negative control without target or with the interferents containing SM, TM, miRNA-144, miRNA-122a, miRNA-32, respectively, showed weak ECL intensity. These results demonstrated that the developed sensing platform had high sequence specificity and base discrimination capability. Briefly, the investigation showed the good selectivity of this strategy for miRNA-21 detection.

The reproducibility, another important indicator, was examined by intra-assay and inter-assay to assess the performance of the proposed method with miRNA-21 standards (0.1 pM). As indicated in Fig. 4(B), the relative standard deviations (RSD) of the prepared ECL sensing system in a single batch (intra-assay) and in various batches (inter-assay) were 3.66% and 4.10%, respectively, suggesting the good analytical reproducibility of the ECL assay.

3.6. Matrix effect and real sample assay

Moreover, the matrix effect was evaluated by comparing the ECL response of the constructed biosensor toward miRNA-21 in buffer 1 as well as in lysates from 10^2 cells of HEK-293, which was low level expression of miRNA-21. As exhibited in Fig. 5(A), the ECL signal responding to lysates of HEL-293 was consistent with that in buffer 1, indicating the good tolerance to matrix effect of the proposed strategy.

To further confirm the practicability and accuracy of this detection method applied in practical cell lines samples, a standard qRT-PCR and the proposed strategy were employed to test the level of miRNA-21 in different cells containing the HEK-293 (a cell line with the low expression of miRNA-21), HeLa cells and MCF-7 (cell lines with upregulated levels of miRNA-21). As shown in Fig. 5(B), the number of copies of miRNA-21 per ng of total RNA determined using the proposed method was similar to that obtained by the qRT-PCR method. Moreover, the results were in accordance with the previous report (He et al., 2016), demonstrating the satisfied accuracy of our strategy, and promising potential in practical application for miRNA detection.

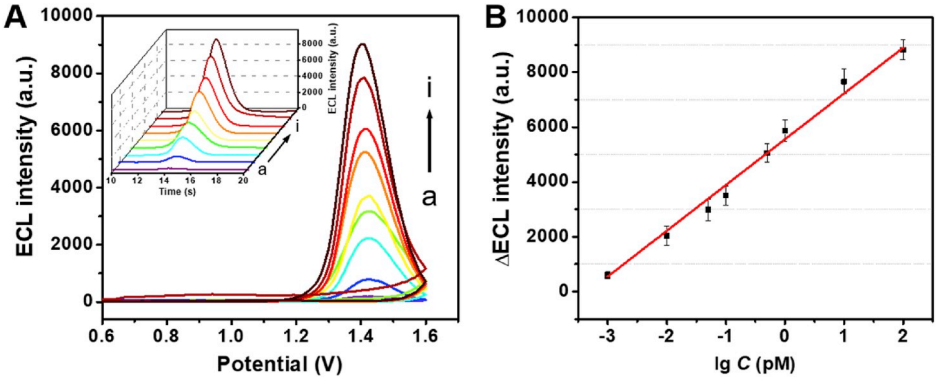

Fig. 3. (A) ECL response at different miRNA-21 concentrations. (a–i) 0, 1.0 fM, 10.0 fM, 50.0 fM, 0.10 pM, 0.50 pM, 1.0 pM, 10.0 pM, 100.0 pM. (B) The calibration curve between *ΔECL* and the logarithm of the miRNA-21 concentration. The error bars represent the standard deviation of three replicate detections.

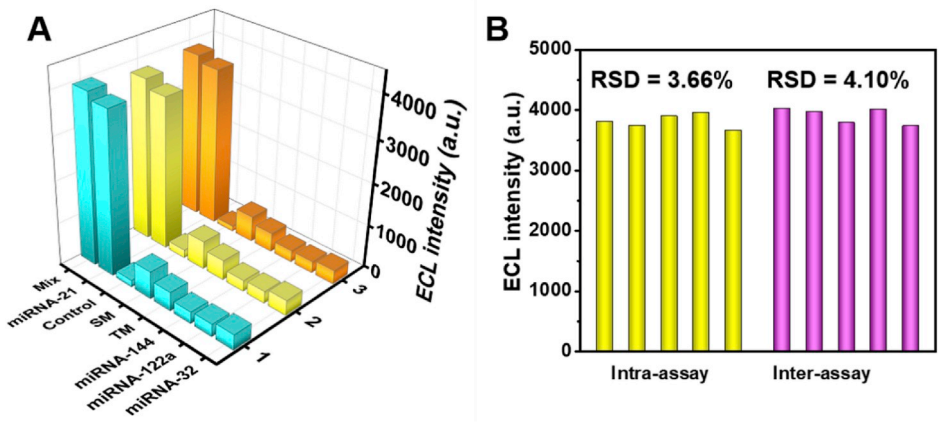

Fig. 4. (A) Selectivity and (B) Reproducibility of the proposed ECL biosensor. The concentration of interferents were set 1.0 pM, and the target miRNA-21 was 0.10 pM.

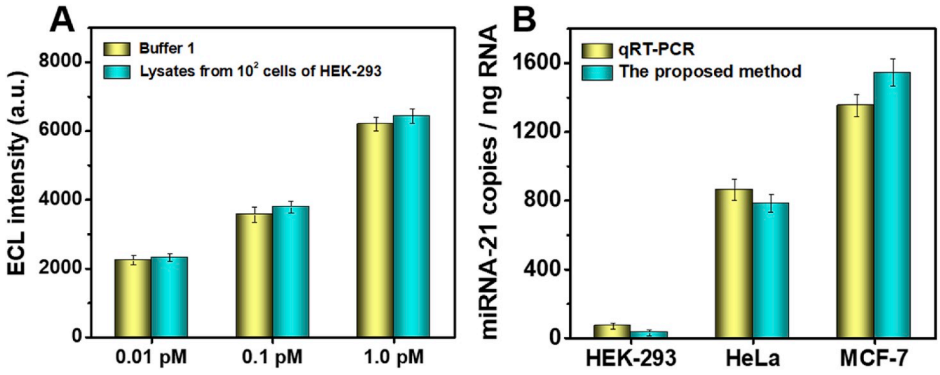

Fig. 5. (A) ECL responses of the proposed biosensor towards 0.01, 0.1, and 1.0 pM miRNA in buffer 1 solution and lysates from 10^2 cells of HEK-293. (B) The number of copies of miRNA-21 per ng RNA determined using our proposed method in HEK-293 cell, HeLa cell and MCF-7 cell compared with the qRT-PCR.

4. Conclusion

In summary, a new high sensitive and selective ECL biosensor consisting of TMSD amplification and NCs–Ru(phen)$_3^{2+}$ as signal tags for miRNA-21 detection was successfully constructed. The introduction of TMSD process exhibited the superb selectivity to discriminate the miRNA family members. Significantly, the converting of single miRNA to lots of ssDNA output was able to amplify signal. Meanwhile, the high loaded capability of DNA NCs with Ru(phen)$_3^{2+}$ resulted in high sensitivity, and the pre-synthesis of NCs–Ru(phen)$_3^{2+}$ with stable ECL properties simplified the operation steps. It also showed good precision and reproducibility. As expected, the well-designed sensing platform was applied to detect miRNA-21 in complex matrix and real samples of cells with good results, which was consistent with the qRT-PCR method. Furthermore, the TMSD amplification is programmable, so the proposed strategy can be used for the assay of some other miRNA by simple sequence design. These results demonstrate that the proposed method holds great potential and broader application in bioanalysis and clinical early diagnosis.

Declaration of competing interest

The authors declare that they have no known competing financial interests or personal relationships that could have appeared to influence the work reported in this paper.

CRediT authorship contribution statement

Ying Zhang: Conceptualization, Investigation, Writing - original draft. **Guoyan Xu:** Conceptualization, Investigation. **Guili Lian:** Data curation, Formal analysis. **Fang Luo:** Methodology, Writing - review & editing. **Qunfang Xie:** Supervision, Writing - review & editing. **Zhenyu Lin:** Funding acquisition, Supervision, Writing - review & editing. **Guonan Chen:** Supervision, Project administration.

Acknowledgements

This project was financially supported by National Natural Science Foundation of China of China (21775026, 21575025, 21575027, 81700267), the Program for Changjiang Scholars and Innovative Research Team in University (No. IRT15R11) and the cooperative project of production and study in University of Fujian Province (2018Y4007), the Sciences Foundation of Fujian Province (2018J01685, 2018J01682), STS Key Project of Fujian Province (2017T3007).

Appendix A. Supplementary data

Supplementary data to this article can be found online at https://doi.org/10.1016/j.bios.2019.111789.

References

Babarniri, B., Bahari, D., Salimi, A., 2019. Biosens. Bioelectron. 142, 111530.
Bartel, D.P., 2004. Cell 116 (2), 281–297.
Cao, J.-T., Liu, F.-R., Fu, X.-L., Ma, J.-X., Ren, S.-W., Liu, Y.-M., 2019. Chem. Commun. 55 (19), 2829–2832.
Cao, J.-T., Wang, Y.-L., Zhang, J.-J., Dong, Y.-X., Liu, F.-R., Ren, S.-W., Liu, Y.-M., 2018. Anal. Chem. 90 (17), 10334–10339.
Chen, Y., Zhou, S., Li, L., Zhu, J.-J., 2017. Nano Today 12, 98–115.

Cheng, Y.Q., Zhang, X., Li, Z.P., Jiao, X.X., Wang, Y.C., Zhang, Y.L., 2009. Angew. Chem. Int. Ed. 48 (18), 3268–3272.
Di Leva, G., Croce, C.M., 2013. Curr. Opin. Genet. Dev. 23 (1), 3–11.
He, L., Hannon, G.J., 2004. Nat. Rev. Genet. 5 (7), 522–531.
He, X., Zeng, T., Li, Z., Wang, G., Ma, N., 2016. Angew. Chem. Int. Ed. 55 (9), 3073–3076.
Kim, E., Zwi-Dantsis, L., Reznikov, N., Hansel, C.S., Agarwal, S., Stevens, M.M., 2017. Adv. Mater. 29 (26), 1701086.
Kulcheski, F.R., Marcelino-Guimaraes, F.C., Nepomuceno, A.L., Abdelnoor, R.V., Margis, R., 2010. Anal. Biochem. 406 (2), 185–192.
Li, L., Chen, Y., Zhu, J.-J., 2017. Anal. Chem. 89 (1), 358–371.
Li, S.-K., Chen, A.-Y., Niu, X.-X., Liu, Z.-T., Du, M., Chai, Y.-Q., Yuan, R., Zhuo, Y., 2017. Chem. Commun. 53 (69), 9624–9627.
Lujambio, A., Lowe, S.W., 2012. Nature 482 (7385), 347–355.
Raymond, C.K., Roberts, B.S., Garrett-Engele, P., Lim, L.P., Johnson, J.M., 2005. RNA-Publ. RNA Soc. 11 (11), 1737–1744.
Rizwan, M., Mohd-Naim, N.F., Ahmed, M.U., 2018. Sensors 18 (1), 166.
Small, E.M., Olson, E.N., 2011. Nature 469 (7330), 336–342.
Srinivas, N., Ouldridge, T.E., Sulc, P., Schaeffer, J.M., Yurke, B., Louis, A.A., Doye, J.P.K., Winfree, E., 2013. Nucleic Acids Res. 41 (22), 10641–10658.
Sun, W.J., Ji, W.Y., Hall, J.M., Hu, Q.Y., Wang, C., Beisel, C.L., Gu, Z., 2015. Angew. Chem. Int. Ed. 54 (41), 12029–12033.
Sun, W.J., Jiang, T.Y., Lu, Y., Reiff, M., Mo, R., Gu, Z., 2014. J. Am. Chem. Soc. 136 (42), 14722–14725.
Wang, C., Sun, W., Wright, G., Wang, A.Z., Gu, Z., 2017. Adv. Mater. 29 (15), 8912–8920.
Wang, G.L., Zhang, C.Y., 2012. Anal. Chem. 84 (16), 7037–7042.
Wang, Y., Jiang, M., Shan, Y., Jin, X., Gong, M., Wang, X., 2018. J. Lumin. 201, 135–142.
Xu, Z., Liao, L., Chai, Y., Wang, H., Yuan, R., 2017. Anal. Chem. 89 (16), 8282–8287.
Yang, L., Tao, Y., Yue, G., Li, R., Qin, B., Guo, L., Lin, Z., Yang, H.-H., 2016. Anal. Chem. 88 (10), 5097–5103.
Yu, Y.Y., Chen, Z.G., Shi, L.J., Yang, F., Pan, J.B., Zhang, B.B., Sun, D.P., 2014. Anal. Chem. 86 (16), 8200–8205.
Zhang, D.Y., Seelig, G., 2011. Nat. Chem. 3 (2), 103.
Zhang, P., Wu, X.Y., Yuan, R., Chai, Y.Q., 2015. Anal. Chem. 87 (6), 3202–3207.
Zhang, Y., Wang, L., Luo, F., Qiu, B., Guo, L., Weng, Z., Lina, Z., Chen, G., 2017. Chem. Commun. 53 (20), 2910–2913.
Zhu, J.B., Zhang, L.B., Li, T., Dong, S.J., Wang, E.K., 2013. Adv. Mater. 25 (17), 2440–2444.
Zhu, S.M., Wu, H.L., Wu, F.T., Nie, D.T., Sheng, S.J., Mo, Y.-Y., 2008. Cell Res. 18, 350–359.